

Electronic and magnetic properties of the 2H-NbS₂ intercalated by 3d transition metal atoms

S. Mankovsky, S. Polesya, and H. Ebert
*Department Chemie, Physikalische Chemie,
 Universität München, Butenandstr. 5-13,
 81377 München, Germany*

W. Bensch
*Inst. für Anorgan. Chemie, Universität Kiel,
 Olshausenstr. 40, 24098 Kiel, Germany*

(Dated: July 21, 2016)

The electronic structure and magnetic properties of the 2H-NbS₂ compound intercalated by Cr, Mn and Fe, have been investigated by means of the Korringa-Kohn-Rostoker (KKR) method. The calculations demonstrate easy plane magneto-crystalline anisotropy (MCA) of Cr_{1/3}NbS₂ monotonously decreasing towards the Curie temperature in line with the experimental results. The modification of the electronic structure results in a change of the easy axis from in-plane to out-of-plane. It is shown, that for Cr_{1/3}NbS₂ and Mn_{1/3}NbS₂ the in-plane MCA and Dzyaloshinskii-Moriya interactions results in a helimagnetic structure along the hexagonal *c* axis, following the experimental observations. The negative exchange interactions in the Fe_{1/3}NbS₂ compound results in a non-collinear frustrated magnetic structure if the MCA is not taken into account. It is shown, however, that a strong MCA along the hexagonal *c* axis leads to a magnetic ordering referred to as an ordering of the third kind, which was observed experimentally.

PACS numbers: Valid PACS appear here

I. INTRODUCTION

The transition metal dichalcogenides (TMDC) are in the focus of extensive investigations for several decades. Although most of TMDC systems are nonmagnetic, they allow intercalation of magnetic 3d elements, *M*, (see, e.g. review article [1]) leading to the formation of materials exhibiting a great variety of magnetic properties dependent on the host system, on the type and concentration of elements *M*. Some examples for this are the large magnetoresistance (MR) in Fe_{0.28}TaS₂ single crystal [2] and the extremely high magnetic anisotropy and anomalous Hall effect (AHE) in Fe_{1/4}TaS₂ [3, 4] recently discussed in the literature. In the present work we will focus on NbS₂ intercalated with Cr, Mn, and Fe. For the concentration 1/3 of the 3d element, these systems exhibit the trend to the formation of an ordered compound, called in the literature either *M*Nb₃S₆ or *M*_{1/3}NbS₂, with an $\sqrt{3} \times \sqrt{3}$ arrangement of the *M* atoms within the layer. If these compounds are magnetically ordered, they show a non-vanishing Dzyaloshinskii-Moriya (DM) interaction because of the lack of inversion symmetry. This anisotropic exchange interaction is in particular responsible for the formation of a helimagnetic (HM) structure under normal conditions. However, an applied external magnetic field leads in some materials to the formation of a complicated magnetic texture as for example skyrmions having nontrivial topological properties [5, 6].

Experimentally, it was observed that the compound Cr_{1/3}NbS₂ is a metallic ferromagnet, with a Curie tem-

perature $T_C = 163$ K and a Cr magnetic moment of $2.9 \mu_B$ [7]. A similar magnitude for the magnetic moment was found also by Miyadai et al.[8], while the Curie temperature reported is somewhat smaller ($T_C = 127$ K). Performing small-angle neutron diffraction measurements, these authors could give evidence for a long-period helimagnetic structure in Cr_{1/3}NbS₂ along the hexagonal *c*-axis, with Cr magnetic moments lying within plane perpendicular to the *c*-axis. These results have been confirmed by other experimental groups by using Lorentz microscopy and small-angle electron diffraction [9], as well as muon spin rotation and relaxation measurements [10]. The experimental investigations using a superconducting quantum interference device (SQUID) magnetometer [11] demonstrated a transition from the commensurate to the incommensurate helimagnetic structure in the presence of a magnetic field directed perpendicular to the hexagonal *c*-axis. A similar behaviour has also been found for Mn_{1/3}NbS₂, although no neutron scattering results are available so far that show explicitly the helimagnetic structure in Mn_{1/3}NbS₂.

The transition from the helimagnetic structure to the state with an incommensurate chiral magnetic soliton lattice (CSL) in Cr_{1/3}NbS₂ in the presence of a magnetic field $\vec{H} \perp c$ has been recently investigated by several groups [9, 12]. They have found that the size and number of magnetic domains in the CSL state, having spin orientation along the magnetic field and separated by 360° domain walls, can be easily manipulated by the magnetic field. This leads in particular to interesting

transport properties in the system, such as a noticeable negative magneto-resistance (MR) along the chiral c axis [5], observed in a wide range of temperature below the incommensurate-commensurate phase transition [12, 13]. Togawa *et al.* [14, 15] demonstrated (using a combination of magneto-transport measurements and Lorentz transmission electron microscopy) the step-wise and hysteretic changes of the MR due to soliton confinement in a small $\text{Cr}_{1/3}\text{NbS}_2$ crystal with the CSL. These properties make $\text{Cr}_{1/3}\text{NbS}_2$ attractive for spintronic applications.

The $\text{Fe}_{1/3}\text{NbS}_2$ compound, in contrast to $\text{Cr}_{1/3}\text{NbS}_2$ and $\text{Mn}_{1/3}\text{NbS}_2$, exhibits antiferromagnetic ordering with the Néel temperature reported to be $T_N = 100$ K [16], 47 K [17], or 44 K [18]. The analysis of magnetic neutron scattering data [16] as well as of Mössbauer spectra [17] suggest a collinear alignment of the Fe magnetic moments along the hexagonal c -axis. So far, however, there are no theoretical investigations on the magnetic structure in this material.

In the present work we present a comparison of magnetic properties of $\text{Cr}_{1/3}\text{NbS}_2$, $\text{Mn}_{1/3}\text{NbS}_2$ and $\text{Fe}_{1/3}\text{NbS}_2$ compounds, obtained within first principles calculations, demonstrating the importance of the relativistic effects for their magnetic properties and discuss the differences between the compounds.

II. COMPUTATIONAL DETAILS

The present investigations on the magnetic properties of NbS_2 intercalated with Cr, Mn, and Fe are based on first-principles electronic structure calculations which have been performed using the fully relativistic KKR Green function method [19, 20]. The calculations have been done in the framework of the local spin density approximation (LSDA) to density functional theory (DFT) using the parametrization for the exchange and correlation potential as given by Vosko *et al.* [21]. For the angular momentum expansion of the Green function a cutoff of $l_{\text{max}} = 3$ was applied.

The magneto-crystalline anisotropy (MCA) at $T = 0$ K was investigated via first-principles calculations of the magnetic torque $\vec{T}_i^{(\hat{e}_i)} = -\partial E(\{\hat{e}_k\})/\partial \hat{e}_i \times \hat{e}_i$ acting on the magnetic moment $\vec{m}_i = m_i \hat{e}_i$ at atomic site i and oriented along the direction of the total magnetization \vec{M} . The torque projection onto the direction \hat{u} , $T_{\hat{u}}(\theta, \phi) = \vec{T}_i^{(\hat{e}_i)} \cdot \hat{u}$, having the form

$$T_{\hat{u}}(\theta, \phi) = -\partial E(\vec{M}(\theta, \phi))/\partial \theta, \quad (1)$$

was calculated for $\phi = 0$ (assuming weak anisotropy within the plane perpendicular to the c axis) and $\theta = \pi/4$, giving immediately the MCA coefficient K_1 [22].

In the case of finite temperature, $T > 0$ K, the torque calculations for $T_{\hat{u}}(\theta = \pi/4)$ have been performed within the relativistic disorder local moment (RDLM) scheme as described by Staunton, *et al.* [22, 23].

In order to investigate the equilibrium magnetic structure and finite temperature magnetic properties of the

	Expt		Theory	
	a	c	a	c
$\text{Cr}_{1/3}\text{NbS}_2$	5.73	12.11	5.782	12.141
$\text{Mn}_{1/3}\text{NbS}_2$	5.779	12.599	5.814	12.378
$\text{Fe}_{1/3}\text{NbS}_2$	5.761	12.178	5.794	12.084

TABLE I. The structure parameters (in Å) for Cr- [7], Mn- [16], and Fe- [16] intercalated NbS_2 for M occupying the (2c) Wyckoff position.

compounds under consideration, Monte Carlo simulations have been performed, which are based on the extended Heisenberg model with the Hamiltonian accounting for relativistic effects and represented by the following expression

$$H = - \sum_{i,j(i \neq j)} \hat{e}_i \underline{J}_{ij} \hat{e}_j + \sum_i K_1 (\hat{e}_i)_z^2. \quad (2)$$

Here K_1 is the uniaxial anisotropy constant and \underline{J}_{ij} is the exchange coupling tensor representing the isotropic exchange interactions $J_{ij} = \frac{1}{3} \text{Tr}(\underline{J}_{ij})$ as well as the components of the DM interactions $D_{ij}^\lambda = \frac{1}{2} \epsilon_{\lambda\mu\nu} (J_{ij}^{\mu\nu} - J_{ij}^{\nu\mu})$ [24].

III. RESULTS

A. Structure

Within the present work we have used structural information taken from experiment [7, 16, 25]. As it was pointed out in these works, the intercalated $M_x\text{NbS}_2$ systems with $M = \text{Cr}$, Mn, and Fe exhibit at $x = 1/3$ a $\sqrt{3} \times \sqrt{3}$ superstructure within the M layers, leading to a well defined ordered compound crystallizing in the space group $P6_322$. This implies an occupation of the (12i) Wyckoff positions (with $x = 1/3, y = 0, z = 3/8$) by S atoms, and occupation of the 2a and 4f (with $z = 0$) positions by Nb atoms. For the M atoms, this symmetry group allows three possible positions: 2b, 2c and 2d. Experimental results, however, suggest the occupation of the 2c position (1/3, 2/3, 1/4) to be most probable. In order to investigate the impact of the optimization of structure parameters via DFT calculations, a corresponding optimization has been performed using the Vienna ab initio simulation package (VASP) [26, 27]. The optimized structure parameters for the compounds with the M atoms occupying the 2c Wyckoff positions are presented in Table I together with the experimental data.

B. Electronic structure

The electronic structure calculations have been performed for the FM state for all systems under consideration. The total spin projected densities of states (DOS),

$n(E)$, are represented in Fig. 1. As one can see, the DOS of the majority-spin states at the Fermi energy E_F is rather large for all compounds. In the case of minority-spin states of $\text{Cr}_{1/3}\text{NbS}_2$ and $\text{Mn}_{1/3}\text{NbS}_2$ one can see a 'pseudogap' between the occupied and unoccupied states with a finite DOS at the Fermi level originating from the d -states of Nb crossing the Fermi level (see the Bloch spectral function (BSF) in Fig. 3). In the case of $\text{Fe}_{1/3}\text{NbS}_2$ the Fermi energy is located at the DOS maximum corresponding to the Fe minority-spin d -states and is finite for both spin directions $n(E_F)$.

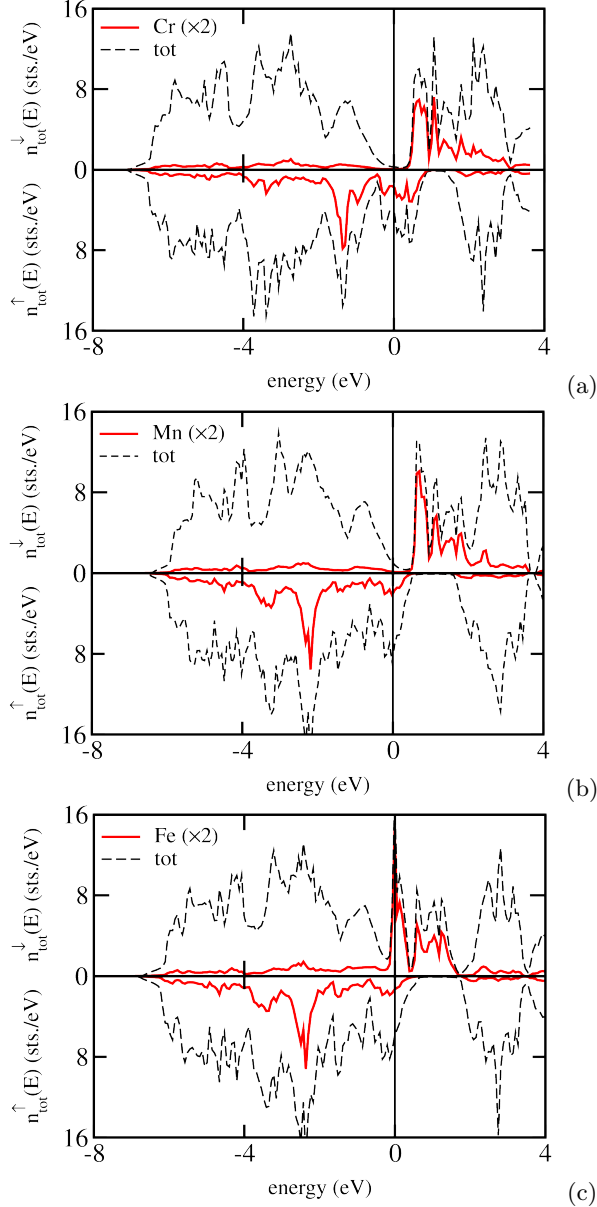


FIG. 1. The total DOS for the FM-ordered $M_{1/3}\text{NbS}_2$ ($M = \text{Cr}, \text{Mn}, \text{Fe}$) together with the partial DOS for the M atom (scaled by the factor of 2).

Table II represents the spin and orbital magnetic moments of the M atoms in comparison with experimental

	m_{spin}	m_{orb}	m_{spin}^o	m_{orb}^o	$m_{\text{spin}}^{\text{expt}}$	E_{MCA}
$\text{Cr}_{1/3}\text{NbS}_2$	2.916	-0.022	2.914	-0.023	2.9	0.21
$\text{Mn}_{1/3}\text{NbS}_2$	3.791	0.014	3.758	0.013	3.8	0.48
$\text{Fe}_{1/3}\text{NbS}_2$	2.905	0.215	2.924	0.210	-	-1.56

TABLE II. Spin and orbital magnetic moments of M atoms in μ_B/atom : present results vs experiment (derived from saturation measurements) [7, 8]. m_{spin}^o and m_{orb}^o represent results obtained using the structure parameters for the optimized structure (see Table I). The calculated MCA energy E_{MCA} is represented in meV/(f.u.). A negative value implies the easy-axis concerning the MCA to be along the c axis.

results derived from measurements of the saturation magnetization [7]. The calculated spin magnetic moments are obviously in good agreement with the experimental data.

One can also see that the Cr and Mn orbital magnetic moments in the corresponding intercalated systems are rather small. In contrast, Fe in $\text{Fe}_{1/3}\text{NbS}_2$ has an orbital magnetic moment that is larger by an order of magnitude. This can be attributed to the narrow-band of the Fe minority-spin d -states at the Fermi energy (see Figs. 1 and 3). In Table II we represent also the spin and orbital magnetic moments obtained for the systems using the optimized structure parameters shown in Table I. As one can see, they are both close to the experimental values as well as to the results obtained for the systems with experimental structure parameters. In the last column of the Table II results for the MCA are shown calculated for the FM ordered $M_{1/3}\text{NbS}_2$ systems for $T = 0$ K. These results imply an uniaxial easy plane anisotropy in the case of $\text{Cr}_{1/3}\text{NbS}_2$ and $\text{Mn}_{1/3}\text{NbS}_2$ and an easy axis along the c axis in the case of $\text{Fe}_{1/3}\text{NbS}_2$, fully in line with experiment. Note also that the magnitude of the MCA in the former cases is much smaller than in the latter one. This can be easily understood by analyzing in detail the electronic structure represented in Figs. 2 and 3. For the case of $\text{Fe}_{1/3}\text{NbS}_2$ the band with minority spin d -character is rather narrow and is located at the Fermi level. This results in a significant contribution to the energy $\sim w^{-1}$ due to SOC splitting of the states having the same spin direction, with the bandwidth w , leading to a preferable magnetization direction along the quantization axis parallel to the hexagonal c axis (see, e.g. the discussions by Wu et al. [28]). In the case of $\text{Cr}_{1/3}\text{NbS}_2$ and $\text{Mn}_{1/3}\text{NbS}_2$ the Fermi level is positioned between the spin-up and spin-down d -bands of the $3d$ metal Cr and Mn, respectively. This results in a significant SOC-induced energy gain associated with the states having opposite spin directions, which competes with the spin-diagonal part of the energy. Using the average exchange splitting Δ_{ex} for the Cr (Mn) d -states, the SOC-induced energy gain for the in-plane orientation of the magnetic moment is $\sim \Delta_{\text{ex}}^{-1}$, which is comparable with the energy gain for \vec{M} oriented along c , and $\sim w_{\text{up}}^{-1}$. As given by Table II these lead for these two compounds to an easy plane MCA. The competition of two contributions to the MCA energy results in a smaller magnitude

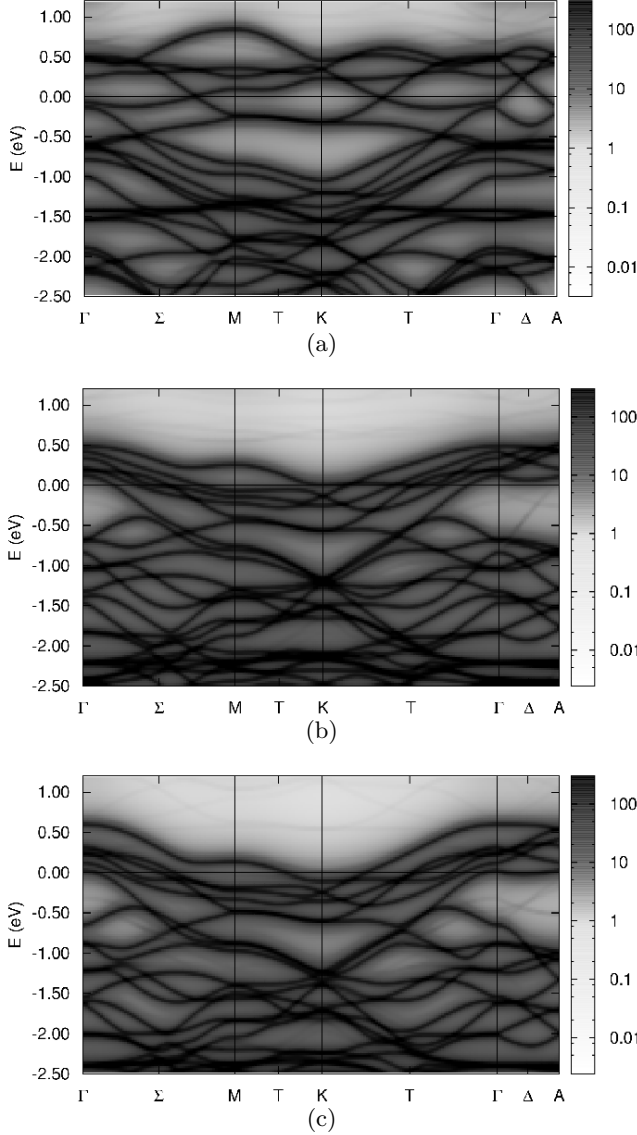


FIG. 2. Spin-up Bloch spectral functions for the FM-ordered $\text{Cr}_{1/3}\text{NbS}_2$ (a) $\text{Mn}_{1/3}\text{NbS}_2$ (b) and $\text{Fe}_{1/3}\text{NbS}_2$ (c), calculated using an imaginary part for the energy of 1 meV.

of MCA of $\text{Cr}_{1/3}\text{NbS}_2$ and $\text{Mn}_{1/3}\text{NbS}_2$ when compared to the $\text{Fe}_{1/3}\text{NbS}_2$.

The temperature dependence of the MCA for $\text{Cr}_{1/3}\text{NbS}_2$ has been investigated within RDLM calculations. Figure 4(a) represents the coefficient of the uniaxial magnetic anisotropy, K_1 , as a function of temperature, in comparison with experimental results. One can see a nearly linear dependence of the MCA energy on the temperature, in full agreement with experiment [8]. Although the calculations underestimate the experiment by about a factor of two, one can nevertheless call the agreement between theory and experiment very satisfying. Figure 4(b) displays also the temperature-dependent variation of the magnetization obtained via RDLM calculations, in comparison with experiment. As one notices,

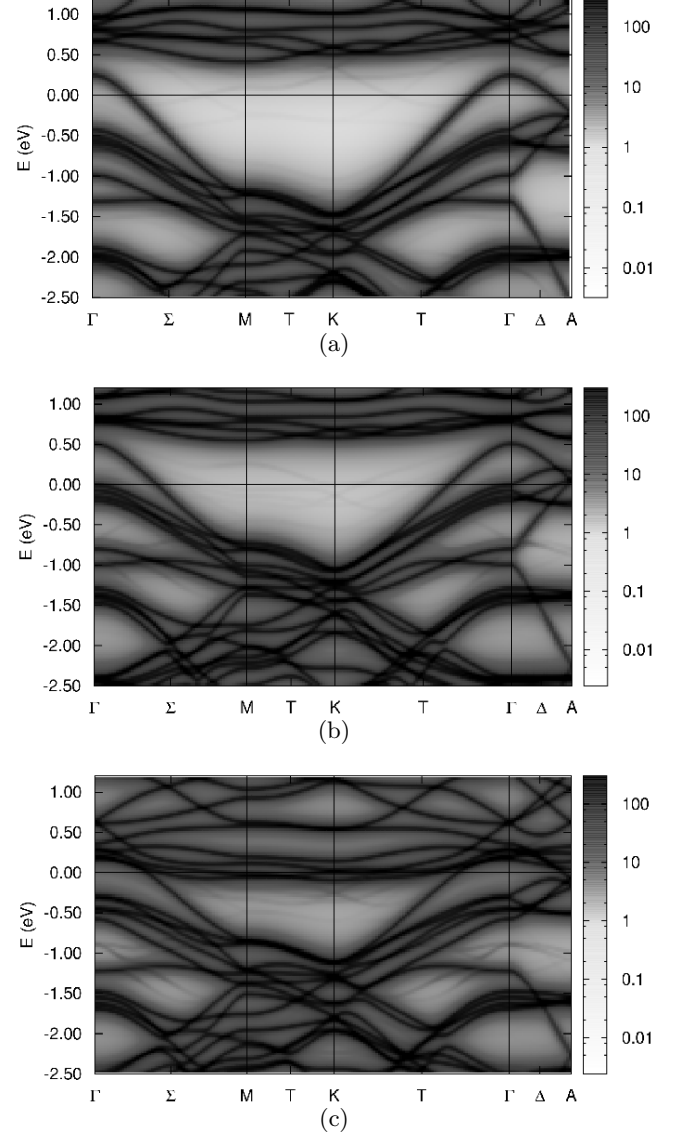


FIG. 3. Spin-down Bloch spectral functions for the FM-ordered $\text{Cr}_{1/3}\text{NbS}_2$ (a) $\text{Mn}_{1/3}\text{NbS}_2$ (b) and $\text{Fe}_{1/3}\text{NbS}_2$ (c), calculated using an imaginary part for the energy of 1 meV.

the theoretical $M(T)$ curve drops faster with increasing T as the experimental one as the RDLM does not include long-range magnetic correlations.

Figure 5 represents the isotropic exchange coupling parameters J_{ij} calculated for all three systems. The strongest magnitude are found for the M - M interactions for the first two neighbour shells. They are predominantly positive for the case of $\text{Cr}_{1/3}\text{NbS}_2$ and $\text{Mn}_{1/3}\text{NbS}_2$ compounds, leading to FM order in these systems when the Dzyaloshinskii-Moriya (DM) interactions are not taken into account. In the case of $\text{Fe}_{1/3}\text{NbS}_2$, however, the Fe-Fe interactions at short distances are negative. Due to the hexagonal crystal structure this should lead to a frustrated magnetic structure. The exchange coupling parameters calculated for the systems with opti-

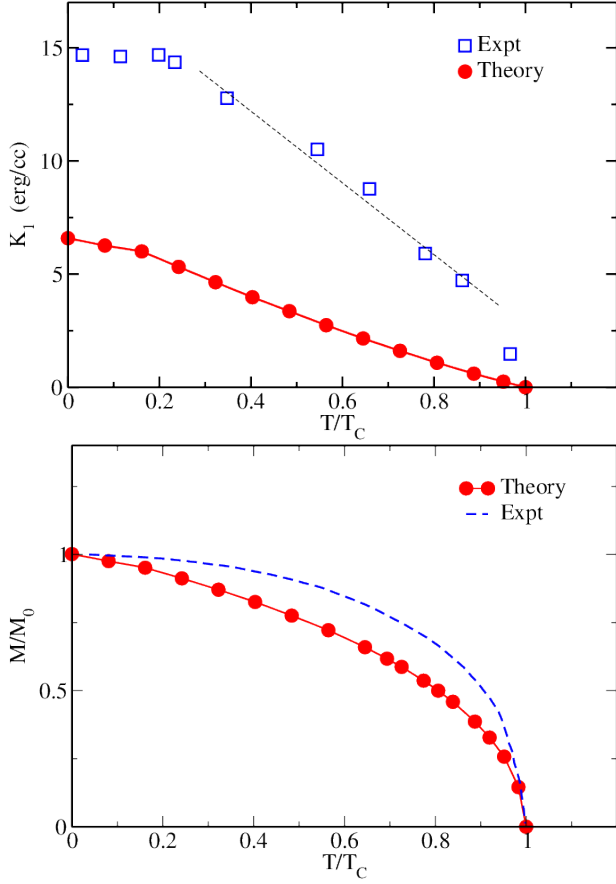


FIG. 4. (a) Magneto-crystalline anisotropy in $\text{Cr}_{1/3}\text{NbS}_2$ as a function of temperature obtained via RDLM selfconsistent calculations in comparison with experimental results [8]. (b) Temperature-dependent variation of the magnetization calculated within the mean field approximation (RDLM scheme) in comparison with the experimental results obtained using the external magnetic field [8].

mized structure parameters are also presented in Fig. 5 (full symbols), demonstrating a rather small difference from the results obtained for experimental structure parameters (open symbols).

The calculated DM interactions for the compounds under discussion, namely the magnitudes and the directions of the DM vectors are shown in Fig. 6. The intralayer DM interactions have the main component along the lines connecting two atoms, with a small z component as shown in Fig. 6(a). One can also see that the weakest interlayer interactions occur for $\text{Cr}_{1/3}\text{NbS}_2$ while the largest for $\text{Fe}_{1/3}\text{NbS}_2$. The same behaviour is found for the D^z components of the DM interactions vector \vec{D} , although the $|D^z|/|\vec{D}|$ ratio decreases in the sequence from $\text{Cr}_{1/3}\text{NbS}_2$ to $\text{Fe}_{1/3}\text{NbS}_2$. Note that the interlayer components D^z are responsible for the formation of a helimagnetic structure along the c axis in $\text{Cr}_{1/3}\text{NbS}_2$. Moreover, their magnitude decrease slowly with distance (see in Fig. 6), while the sign changes from shell to shell. Therefore, the period of the HM structure is determined

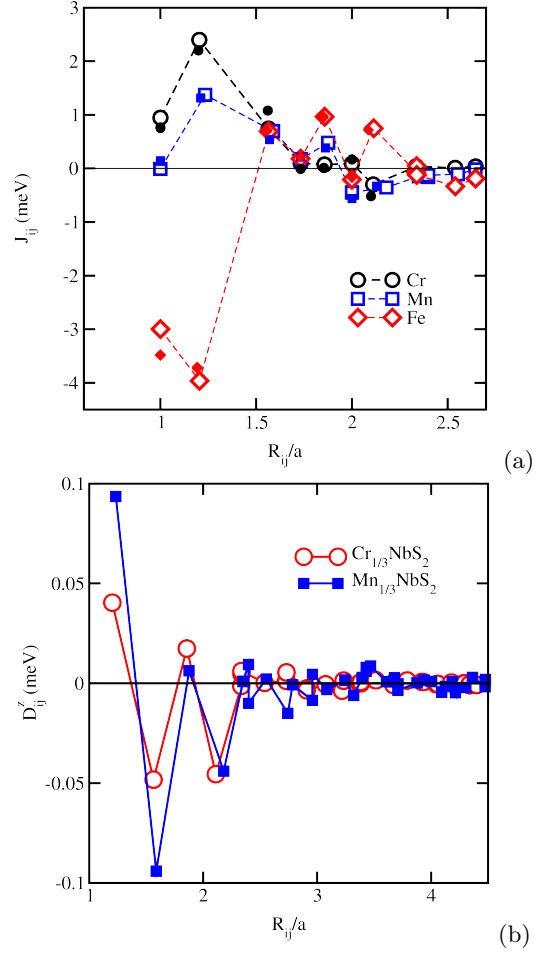


FIG. 5. (a) Isotropic exchange coupling parameters for $M_{1/3}\text{NbS}_2$ ($M = \text{Cr}, \text{Mn}, \text{Fe}$). Open symbols represent results obtained for the experimental structure parameters, full symbols correspond to the systems with the DFT-optimized structure parameters. (b) The D^z component of the DM interactions of Cr and Mn atoms with the neighbours arranged within the layers corresponding to the bottom half-space of the system.

by the DM interactions of Cr atoms which belong at least to several neighboring shells where the DM interactions are non-negligible.

The calculated isotropic exchange parameters, DM interactions and the anisotropy constant K_1 have been used as input for the MC simulations. As it was pointed out above, the FM order has been obtained in the case of $\text{Cr}_{1/3}\text{NbS}_2$ and $\text{Mn}_{1/3}\text{NbS}_2$ compounds and the non-collinear AFM order in the case of $\text{Fe}_{1/3}\text{NbS}_2$, when the DM interactions were not taken into account. The calculated critical temperatures are listed in Table III in comparison with the experimental results demonstrating rather good agreement.

The interplay of the in-plane MCA and of the DM interactions (namely, D^z component) in $\text{Cr}_{1/3}\text{NbS}_2$ result in a long-period helimagnetic structure represented by the in-plane Cr magnetic moments twisted around the c

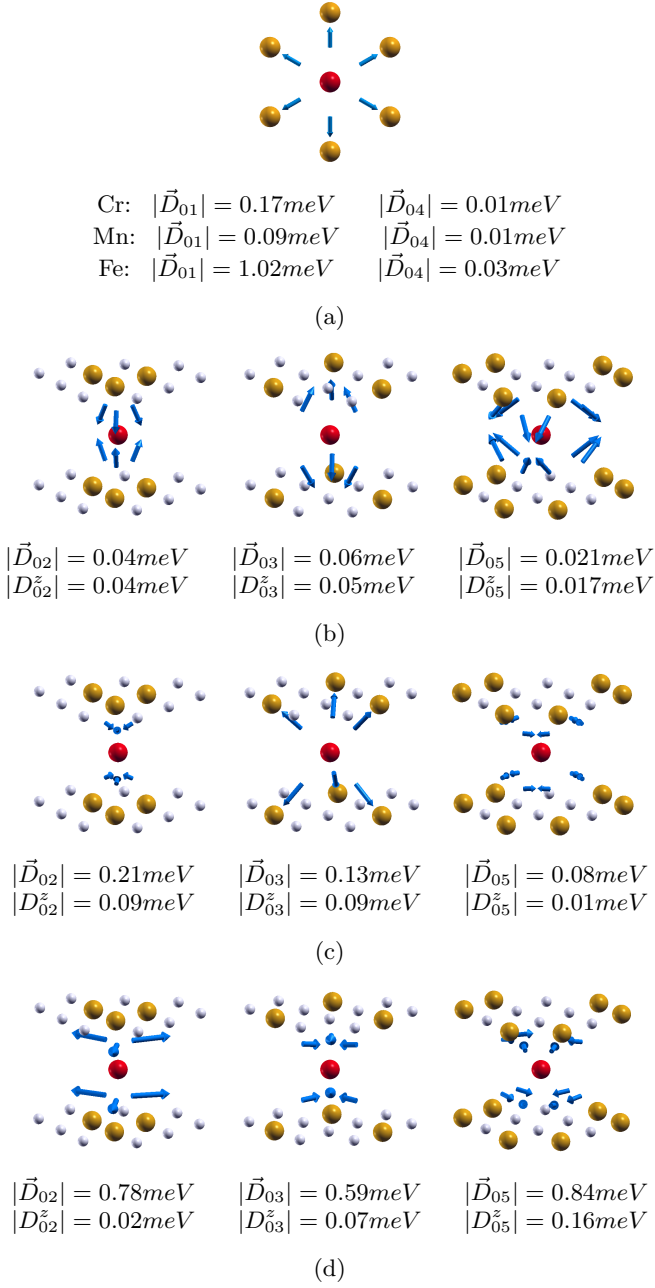


FIG. 6. (a) Dzyaloshinskii-Moriya exchange coupling parameters shown schematically for all $M_{1/3}\text{NbS}_2$, between the first \vec{D}_{01} and second \vec{D}_{04} neighbors within the M plane. DM interactions between the M atoms corresponding to different neighboring planes: (b) for $\text{Cr}_{1/3}\text{NbS}_2$, (b) $\text{Mn}_{1/3}\text{NbS}_2$ and (c) $\text{Fe}_{1/3}\text{NbS}_2$.

axis as it is shown by the snapshot in Fig. 7 obtained from MC simulations. Note that this result is obtained accounting only the first two neighbour shells. In this case, the period of the HM order is of $\sim 340a$ where a is the lattice parameter, that significantly overestimates the HM period observed experimentally ~ 46 nm, or $\sim 86a$, respectively, [9]. The simple evaluation accounting for

	MC	RDLM	EXPT
$\text{Cr}_{1/3}\text{NbS}_2$	115(FM)	310(FM)	127(FM) [8]
$\text{Mn}_{1/3}\text{NbS}_2$	80(FM)	170(FM)	65(FM)
$\text{Fe}_{1/3}\text{NbS}_2$	63(AFM)	-	47(AFM)[17], 44(AFM)[18]

TABLE III. The Curie and Néel temperatures (in K units) calculated for $M_{1/3}\text{NbS}_2$ compounds via MC simulations and RDLM selfconsistent calculations, in comparison with experimental results.

nearest neighbour interactions only gives a period similar to that obtained via MC simulations, $2\pi a \frac{D_{02}^z}{J_{02}} = 375a$. To calculate the magnetic structure more accurately, one has to take into account the exchange interactions within the sphere of $4a$ because of the oscillating behaviour of the D^z component of the DM interactions shown in Fig. 5(b)). A simple estimate leads to a HM period of $500a$, i.e. much longer than the experimental value. A similar trend was also obtained for $\text{Mn}_{1/3}\text{NbS}_2$. From these one can conclude that the DM interactions calculated in the work are essentially underestimated. This behaviour correlates with the results for the MCA that is also too low when compared to the experiment. This can presumably be attributed to the approximation used for the exchange-correlation functional. In the present work the LSDA was used, while use of the LSDA+U scheme could be more suitable to get better agreement with the experiment, as for example in the case of MCA calculated for $\text{Fe}_{1/4}\text{TaS}_2$ system [29].

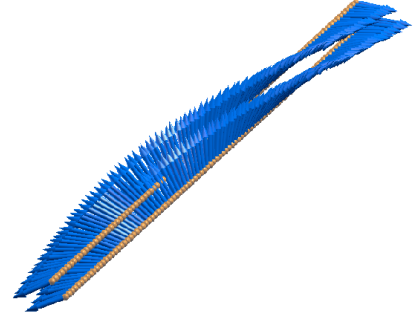


FIG. 7. Helimagnetic structure along c axis in $\text{Cr}_{1/3}\text{NbS}_2$ at $T = 1.0$ K.

In the case of $\text{Mn}_{1/3}\text{NbS}_2$ no direct observations of the helimagnetic structure have been reported, although, the transition to such a state has been observed [11]. This property can be associated with a rather long period of the helimagnetic structure caused by the oscillating behaviour of the D^z component of the DM interactions (see Figs. 5(b)), that can lead to some problems concerning its experimental observations.

For the case of $\text{Fe}_{1/3}\text{NbS}_2$, first of all, the isotropic exchange interaction between the first and second neighbors are negative making their antiparallel alignment preferable. However, due to the hexagonal crystal structure, a competition of the AFM interactions between the neighboring atoms results in a frustrated non-collinear mag-

netic structure in the system. Fig. 8(a) represents the magnetic structure obtained within the MC simulations ($T = 1$ K) neglecting DM interactions. Although the D^z components of the DM vectors are much smaller than two others, D^x and D^y , the DM interactions result in the formation of a chiral spin-spiral structure in $\text{Fe}_{1/3}\text{NbS}_2$ along x , y as well as z directions with a rotation angle of 90° between neighboring atoms along each direction (see Fig. 8(b)).

It should be noted that in experiment [16, 17] a collinear ferrimagnetic structure is formed for $\text{Fe}_{1/3}\text{NbS}_2$, in contradiction to the present calculations. A reason for this discrepancy may be attributed to the magnetic anisotropy along the hexagonal c axis, which has not been taken into account within the calculations shown in Fig. 8(a) and (b). According to the MC simulations based on the Heisenberg model, the calculated K_1 parameter for the magnetic anisotropy represented in Table II, $K_1 = 0.79$ meV/(Fe atom), is still too small to force the system to a collinear state. However, imposing a stronger MCA with $K_1 = 4$ meV/(Fe atom), the magnetic moments are almost perfectly aligned along the c axis, as it is shown in Fig. 8(c). Note that the latter results were obtained for the temperature 4 K, to follow the experimental conditions [16, 17], leading to a finite amplitude of thermal fluctuations. The magnetic structure shown in Fig. 8(c) with the so-called ordering of the third kind [30], is in full agreement with experiment. This implies an antiferromagnetic ordering of each Fe atom with its 12 neighbors such that four of them have their magnetic moments in the same direction and the other 8 atoms in the opposite direction, as a result of the competition of their AFM exchange coupling and uniaxial MCA along the c axis. Although, no experimental results on the MCA are available, the present results allow us to conclude about the underestimated MCA in our calculations, as it was already shown for $\text{Cr}_{1/3}\text{NbS}_2$. Despite this, one can see rather good agreement between theory and experiment, that gives access to the understanding of the origin of magnetic structures and magnetic properties of the systems under consideration.

IV. SUMMARY

In summary, first principles calculations for the exchange coupling, DM interaction and MCA parameters have been performed for Cr-, Mn- and Fe-intercalated NbS_2 . The FM interactions, finite values of the D^z in-

teraction terms and the in-plane MCA in $\text{Cr}_{1/3}\text{NbS}_2$ lead to a helimagnetic structure along the hexagonal c axis, in full agreement with experiment. Similar properties have been obtained also for $\text{Mn}_{1/3}\text{NbS}_2$. No direct experimental observation of the HM structure in $\text{Mn}_{1/3}\text{NbS}_2$ has been done so far, that can be attributed to its long period due to oscillating behaviour of the DM interactions with a distance. In the case of the $\text{Fe}_{1/3}\text{NbS}_2$ compound, a frustrated non-collinear magnetic structure has been found

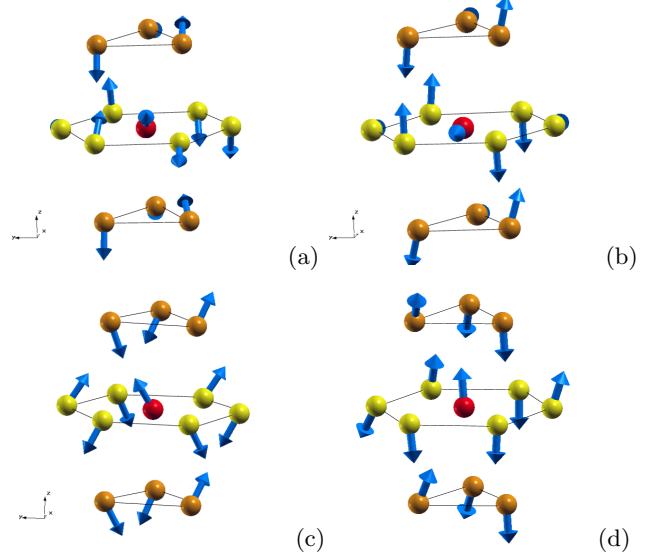


FIG. 8. Magnetic structure in $\text{Fe}_{1/3}\text{NbS}_2$ at $T = 1$ K: (a) DM interactions and MCA are not taken into account; (b) accounting for DM interactions, but without account of MCA; (c) accounting for DM interactions, with calculated MCA coefficient $K_1 = -0.78$ meV/Fe; (d) accounting for DM interactions, with MCA coefficient $K_1 = -4.0$ meV/Fe, and temperature $T = 4$ K.

in the present calculations when the MCA is neglected. However, a strong MCA along the hexagonal c axis leads to the magnetic structure referred to as an ordering of the third kind, being a consequence of a modification of the frustrated non-collinear magnetic structure in the presence of strong MCA.

ACKNOWLEDGMENTS

Financial support by the Deutsche Forschungsgemeinschaft (DFG) via the priority programs SPP 1415 is acknowledged.

- [1] R. Friend and A. Yoffe, *Advances in Physics* **36**, 1 (1987), <http://dx.doi.org/10.1080/00018738700101951>.
- [2] W. J. Hardy, C.-W. Chen, A. Marcinkova, H. Ji, J. Sinova, D. Natelson, and E. Morosan, *Phys. Rev. B* **91**, 054426 (2015).

- [3] J. G. Checkelsky, M. Lee, E. Morosan, R. J. Cava, and N. P. Ong, *Phys. Rev. B* **77**, 014433 (2008).
- [4] Choi, Y. J., Kim, S. B., Asada, T., Park, S., Wu, Weida, Horibe, Y., and Cheong, S-W., *EPL* **86**, 37012 (2009).

- [5] M. N. Wilson, E. A. Karhu, D. P. Lake, A. S. Quigley, S. Meynell, A. N. Bogdanov, H. Fritzsche, U. K. Rößler, and T. L. Monchesky, *Phys. Rev. B* **88**, 214420 (2013).
- [6] A. Bogdanov and A. Hubert, *J. Magn. Magn. Materials* **138**, 255 (1994).
- [7] F. Hulliger and E. Pobitschka, *Journal of Solid State Chemistry* **1**, 117 (1970).
- [8] T. Miyadai, K. Kikuchi, H. Kondo, S. Sakka, M. Arai, and Y. Ishikawa, *Journal of the Physical Society of Japan* **52**, 1394 (1983), <http://dx.doi.org/10.1143/JPSJ.52.1394>.
- [9] Y. Togawa, T. Koyama, K. Takayanagi, S. Mori, Y. Kousaka, J. Akimitsu, S. Nishihara, K. Inoue, A. S. Ovchinnikov, and J. Kishine, *Phys. Rev. Lett.* **108**, 107202 (2012).
- [10] D. Braam, C. Gomez, S. Tezok, E. V. L. de Mello, L. Li, D. Mandrus, H.-Y. Kee, and J. E. Sonier, *Phys. Rev. B* **91**, 144407 (2015).
- [11] Y. Kousaka, Y. Nakao, J. Kishine, M. Akita, K. Inoue, and J. Akimitsu, *Nuclear Instruments and Methods in Physics Research A* **600**, 250 (2009).
- [12] Y. Togawa, Y. Kousaka, S. Nishihara, K. Inoue, J. Akimitsu, A. S. Ovchinnikov, and J. Kishine, *Phys. Rev. Lett.* **111**, 197204 (2013).
- [13] A. X. Gray, J. Minr, L. Plucinski, M. Huijben, A. Bostwick, E. Rotenberg, S. Yang, J. Braun, A. Winkelmann, G. Conti, D. Eiteneer, A. Rattanachata, A. A. Greer, J. Ciston, C. Ophus, G. Rijnders, D. H. A. Blank, D. Doennig, R. Pentcheva, J. B. Kortright, C. M. Schneider, H. Ebert, and C. S. Fadley, *Europhys. Lett.* **104**, 17004 (2013).
- [14] Y. Togawa, T. Koyama, Y. Nishimori, Y. Matsumoto, S. McVitie, D. McGrouther, R. L. Stamps, Y. Kousaka, J. Akimitsu, S. Nishihara, K. Inoue, I. G. Bostrem, V. E. Sinitsyn, A. S. Ovchinnikov, and J. Kishine, *Phys. Rev. B* **92**, 220412 (2015).
- [15] K. Tsuruta, M. Mito, Y. Kousaka, J. Akimitsu, J. ichiro Kishine, Y. Togawa, H. Ohsumi, and K. Inoue, *Journal of the Physical Society of Japan* **85**, 013707 (2016), <http://dx.doi.org/10.7566/JPSJ.85.013707>.
- [16] B. V. Laar, H. Rietveld, and D. Ijdo, *Journal of Solid State Chemistry* **3**, 154 (1971).
- [17] O. Gorocho, A. L. Blanc-soreau, J. Rouxel, P. Imbert, and G. Jehanno, *Philosophical Magazine Part B* **43**, 621 (1981), <http://dx.doi.org/10.1080/01418638108222164>.
- [18] Y. Yamamura, S. Moriyama, T. Tsuji, Y. Iwasa, M. Koyano, S. Katayama, and M. Ito, *Journal of Alloys and Compounds* **383**, 338 (2004), proceedings of the 14th International Conference on Solid Compounds of Transition Elements (SCTE 2003).
- [19] H. Ebert et al., *The Munich SPR-KKR package*, version 6.3, H. Ebert et al. <http://olymp.cup.uni-muenchen.de/ak/ebert/SPRKKR> (2012).
- [20] H. Ebert, D. Ködderitzsch, and J. Minár, *Rep. Prog. Phys.* **74**, 096501 (2011).
- [21] S. H. Vosko, L. Wilk, and M. Nusair, *Can. J. Phys.* **58**, 1200 (1980), <http://www.nrcresearchpress.com/doi/pdf/10.1139/p80-159>.
- [22] J. B. Staunton, L. Szunyogh, A. Buruzs, B. L. Gyorffy, S. Ostanin, and L. Udvardi, *Phys. Rev. B* **74**, 144411 (2006).
- [23] B. L. Gyorffy, A. J. Pindor, J. Staunton, G. M. Stocks, and H. Winter, *J. Phys. F: Met. Phys.* **15**, 1337 (1985).
- [24] H. Ebert and S. Mankovsky, *Phys. Rev. B* **79**, 045209 (2009).
- [25] J. van den Berg and P. Cossee, *Inorganica Chimica Acta* **2**, 143 (1968).
- [26] G. Kresse and J. Furthmüller, *Phys. Rev. B* **54**, 11169 (1996).
- [27] G. Kresse and J. Furthmüller, *Computational Materials Science* **6**, 15 (1996).
- [28] R. Wu, D. Wang, and A. J. Freeman, *Phys. Rev. Lett.* **71**, 3581 (1993).
- [29] S. Mankovsky, K. Chadova, D. Ködderitzsch, J. Minár, H. Ebert, and W. Bensch, *Phys. Rev. B* **92**, 144413 (2015).
- [30] P. W. Anderson, *Phys. Rev.* **79**, 705 (1950).